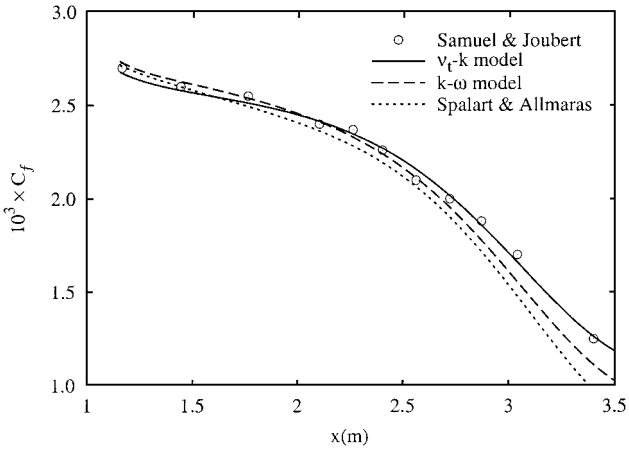

Fig. 2 Friction coefficient in Samuel–Joubert[15] flows.

a fully developed two-dimensional channel flow at $Re_\tau = 395$ (Ref. 13), a flat plate boundary-layer flow,[14] and the boundary-layer flow under adverse pressure gradient.[15]

Applications

Figure 1 shows the comparisons of the predicted U^+, $-\overline{uv}^+$, and k^+ using various models with DNS data. The one-equation model of Spalart and Allmaras[6] and the two-equation model of Wilcox[9] produce slightly larger Reynolds shear stress in the buffer layer, which results in lower velocity profiles in that region. It can be seen that the proposed ν_t–k model yields correct near-wall behavior of the Reynolds shear stress and, thus, the eddy viscosity. Note that other models predict $-\overline{uv}^+ \propto y^4$ as $y \to 0$. The present model is applied to a flat plate boundary layer, which results in good prediction of friction coefficients. A relation, $l = \nu_t/\sqrt{k}$, can infer the turbulence length scale from the ν_t–k model, and it can be seen that the length scale l varies smoothly from zero at the wall to a value in the core region that is similar to that of the conventional algebraic model. For all models considered in this study, the computed skin friction was affected by the location of the first grid point, y_1^+. A comparison of such an influence between k–ε (Ref. 16) and ν_t–k models revealed that a twice larger value of y_1^+ can be used in the ν_t–k model to produce the skin friction within $\pm 1\%$ variation.

Finally, the adverse pressure gradient flow of Samuel and Joubert[15] has been computed. Figure 2 shows that the ν_t–k model best predicts skin-friction coefficients in adverse pressure gradients flows. The predicted velocity and the Reynolds stress profiles, which are not shown here, were also comparable with the experiment.

Conclusions

A new eddy viscosity transport equation is developed to constitute a new ν_t–k model. Natural wall boundary conditions can be used for both ν_t and k equations. Although this model is not free from defects due to the Boussinesq approximation, it yields favorable predictions of a number of standard attached turbulent boundary-layer flows. Further studies are in process to verify the present model for separated flows and compressible flows.

Acknowledgment

This work was supported by a grant from the National Research Laboratory of the Ministry of Science and Technology, Republic of Korea.

References

[1]Baldwin, B. S., and Lomax, H., "Thin-Layer Approximation and Algebraic Model for Separated Turbulent Flows," AIAA Paper 78-257, 1978.

[2]Bradshaw, P., Ferriss, D. H., and Atwell, N. P., "Calculation of Boundary-Layer Development Using the Turbulent Energy Equation," *Journal of Fluid Mechanics*, Vol. 28, 1967, pp. 593–616.

[3]Jones, W. P., and Launder, B. E., "The Prediction of Laminarization with a Two-Equation Model of Turbulence," *International Journal of Heat and Mass Transfer*, Vol. 15, No. 2, 1972, pp. 301–314.

[4]Wilcox, D. C., "Reassessment of the Scale-Determining Equation for Advanced Turbulence Models," *AIAA Journal*, Vol. 26, No. 11, 1988, pp. 1299–1310.

[5]Baldwin, B. S., and Barth, T. J., "A One-Equation Turbulence Transport Model for High Reynolds Number Wall-Bounded Flows," NASA TM-102847, 1990.

[6]Spalart, P. R., and Allmaras, S. R., "A One-Equation Turbulence Model for Aerodynamic Flows," *La Recherche Aérospatiale*, No. 1, 1994, pp. 5–21.

[7]Durbin, P. A., Mansour, N. N., and Yang, Z., "Eddy Viscosity Transport Model for Turbulent Flow," *Physics of Fluids*, Vol. 6, No. 2, 1994, pp. 1007–1015.

[8]Menter, F. R., "Eddy Viscosity Transport Equations and Their Relation to the k–ε Model," *Journal of Fluids Engineering*, Vol. 119, Dec. 1997, pp. 876–884.

[9]Wilcox, D. C., *Turbulence Modeling for CFD*, 2nd ed., DCW Industries, Inc., La Cañada, CA, 1998, pp. 117–149.

[10]Tarvoularis, S., and Karnik, U., "Further Experiments on the Evolution of Turbulent Stresses and Scales in Uniformly Sheared Turbulence," *Journal of Fluid Mechanics*, Vol. 204, 1989, pp. 457–478.

[11]Cazalbou, J. B., Spalart, P. R., and Bradshaw, P., "On the Behavior of Two-Equation Models at the Edge of a Turbulent Region," *Physics of Fluids*, Vol. 6, No. 5, 1994, pp. 1797–1804.

[12]Briggs, D. A., Ferziger, J. H., Koseff, J. R., and Monismith, S. G., "Entrainment in a Shear-Free Turbulent Mixing Layer," *Journal of Fluid Mechanics*, Vol. 310, 1996, pp. 215–241.

[13]Kim, J., Moin, P., and Moser, R., "Turbulence Statistics in Fully Developed Channel Flow at Low Reynolds Number," *Journal of Fluid Mechanics*, Vol. 177, 1987, pp. 133–166.

[14]Kline, S. J., Cantwell, B. J., and Lilley, G. M., *1980-1981 AFOSR-HTTM-Stanford Conference on Complex Turbulent Flows: Comparison of Computation and Experiment*, Stanford Univ., Stanford, CA, 1981, pp. 82–85.

[15]Samuel, A. E., and Joubert, P. N., "A Boundary Layer Developing in an Increasingly Adverse Pressure Gradient," *Journal of Fluid Mechanics*, Vol. 66, 1974, pp. 481–505.

[16]Nagano, Y., and Tagawa, M., "An Improved k–ε Model for Boundary Layer Flows," *Journal of Fluid Engineering*, Vol. 112, 1990, pp. 33–39.

R. M. C. So
Associate Editor

Structural Damage Identification Using Pole/Zero Dynamics in Neural Networks

S. M. Yang* and G. S. Lee†
National Cheng-Kung University, Tainan 701, Taiwan, Republic of China

I. Introduction

EFFECTIVE damage detection and/or identification of structure systems has been the subject of recent studies. The concept is based on that when a structure system undergoes different kinds or degrees of damage, its characteristics will change. A set of structural signatures can then be applied to characterize the damage condition(s). Structural damage identification by artificial neural networks has proven preferable over traditional model-based schemes because of the neural networks, advantages in self-learning, noise insensitivity, fault tolerance, and generalization ability. A feedforward neural network usually has three layers: the input layer, hidden layer, and output layer. From the viewpoint of pattern recognition, a diagnosis network that avoids the complicated algorithms in traditional model-based schemes can construct the mapping of the structural signatures and damage condition. In addition, once an artificial neural network is constructed, it can provide damage identification fast enough for online monitoring.

Received 30 June 1997; revision received 16 April 2001; accepted for publication 26 April 2001.

*Professor, Institute of Aeronautics and Astronautics; smy@mail.iaa.ncku.edu.tw.

†Research Assistant, Institute of Aeronautics and Astronautics.

There have been many studies of structural damage identification by neural networks in the literature. Some used the structural signature of static displacement and mechanical strain under prescribed loads[1–5] as the input patterns of neural networks. Others used the change in displacement- and strain-mode shapes.[6] Time-domain vibration signals[7–9] and the coefficients of the transfer function[10] have also been used as input patterns in the neural-based structural diagnosis system. It is known that the change of structural stiffness is the primary cause of the change of natural frequencies. Tsou and Shen[11] also utilized the change of eigenvalues and mode shapes of a discrete structure system to identify the damage location and extent through a neural network. The mode shape measurement at thousands of nodes of a finite element model is, however, infeasible.

One intuitive and feasible way is by using the change of the natural frequencies to characterize the damage condition(s). Kirkegaard and Rytter,[12] Islam and Craig,[13] Kaminski,[14] and Ferregut et al.[15] used the structural natural frequencies as the neural network input to detect damage conditions. However, structural damage identification by the use of the changes of natural frequencies is an inverse problem. The question is, will two different damage conditions lead to the same natural frequency changes?

An improved method of structural damage identification, utilizing not only the change of natural frequencies (poles) but also the change of zeros, is developed in this Note. The backpropagation neural network with a momentum term and an adaptive learning rate is employed to construct the complex effect-to-cause mapping between the pole/zero dynamics and the damage conditions. Analyses show that this method can effectively identify the extent and location of complex damage conditions.

II. Damage Detection by Use of the Change of Natural Frequencies

A simple three-degree-of-freedom (DOF) spring–mass system shown in Fig. 1 is used to investigate the uniqueness of mapping between the change of natural frequencies and the damage conditions. For a given set of stiffness, the set of three natural frequencies can be determined uniquely because this is inherently a direct process from cause to effect. However, the reverse is not necessarily true. There exist two different damage conditions producing exactly the same set of changes of the natural frequencies. If damage is defined by the degradation of spring stiffness, $[k_1', k_2', k_3']$ denotes the remaining spring stiffness in percentage. Conditions 1 and 2 in Table 1 illustrate that the damage condition of [10%, 30%, 20%] and [60%, 10%, 10%] lead to the same characteristic equation; hence, they have the same change of natural frequencies. There also exist many damage conditions that produce a very similar change of natural frequencies, as shown by conditions 3 and 4. Such a natural frequency difference is difficult, if not impossible, to observe numerically or experimentally. This simple example typifies the deficiency of using the natural frequencies for structural damage identification because they often generate ambiguous damage conditions.

To overcome the given deficiency, one can use the entire frequency spectrum to identify the damage conditions, but the small sampling rate and the associated large data points make the structural diagnosis difficult and impractical. An alternative is to use the change of mode shapes in addition to the natural frequencies for structural damage identification; however, the accuracy requirement of mode shape measurements is more demanding than that of natural frequency measurements. Furthermore, the number of measurements required for constructing mode shapes make this approach impractical in engineering applications.

Table 1 Change of natural frequencies from different damage conditions

Condition	Damage condition $[k_1', k_2', k_3']$	Change of ω, rad/s $[\Delta\omega_1, \Delta\omega_2, \Delta\omega_3]$
1	[10%, 30%, 20%]	[2.113, 6.981, 8.694]
2	[60%, 10%, 10%]	[2.113, 6.981, 8.694]
3	[30%, 30%, 80%]	[1.478, 4.456, 4.187]
4	[20%, 70%, 50%]	[1.508, 4.449, 4.186]

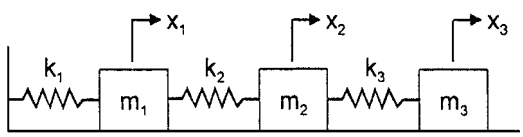

Fig. 1 Spring–mass system.

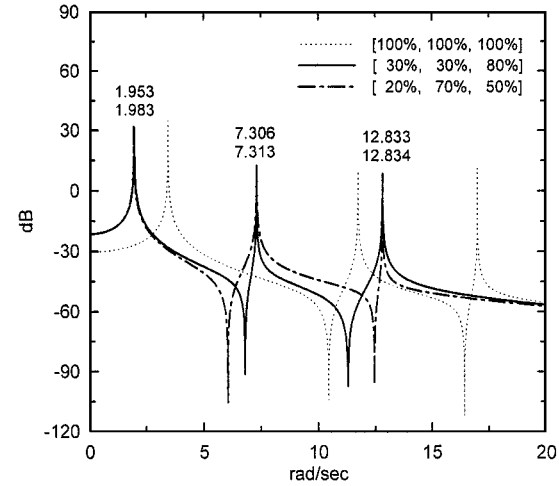

Fig. 2 FRF of spring–mass system under three damage conditions.

Note that the system poles (resonances) and zeros (antiresonances) represent the system dynamics under a certain input–output relation. Figure 2 shows that, although the point frequency response function (FRF) measured at x_3 has almost the same poles in damage conditions 3 and 4, there remains a substantial difference at the frequencies between two adjacent poles. A point FRF is a collocated transfer function where the response measurement and the excitation input are at the same location and there is a zero between two poles. Utilizing the change of both system poles and zeros for structural damage identification may avoid the nonunique mapping of the damage conditions as shown in Table 1. Note that the poles are the characteristics of the system that is independent of measurement location except at the node point. However, the zeros are the local features that are dependent on measurement locations. One has the option of selecting one or a few measurement locations to acquire adequately the change of poles and zeros for structure damage identification.

III. Damage Identification by Neural Networks

A three-layer backpropagation neural network[2,16] is employed to construct the complex effect-to-cause mapping between the change of system pole/zero and damage conditions. The neural network with one hidden layer is denoted by $[x–y–z]$ to represent the network of x input neurons, y hidden layer neurons, and z output neurons. The activation functions in the hidden and output neurons are the hyperbolic-tangent functions with the output range $(-1, 1)$ and the sigmoidal function with the output range $(0, 1)$, respectively. The number of poles and zeros required to identify different damage conditions determines the number of input neurons. Each output neuron represents a possibly damaged stiffness member of the structure. The poles and zeros of the system in Fig. 1 are well separated. There are, however, systems with closely spaced natural frequencies whose damage identification becomes more challenging. Kabe's spring mass model,[17] as shown in Fig. 3, is an eight-DOF spring–mass system with closely spaced natural frequencies. The system dynamics can be illustrated by the FRF at m_6 as shown in Fig. 4, where ω_2 and ω_3 are too close to be identified. In addition, ω_7 is unobservable because the associated eigenvector component is nearly zero. It is assumed that the damage occurs only at six main springs with higher stiffnesses, that is, at k_2, k_4, k_6, k_8, k_{10}, and k_{12}.

Consider three stiffness damages at a time, each losing its stiffness from 10 to 40% with a 10% interval simulating the damage. The training data for the diagnosis network were collected

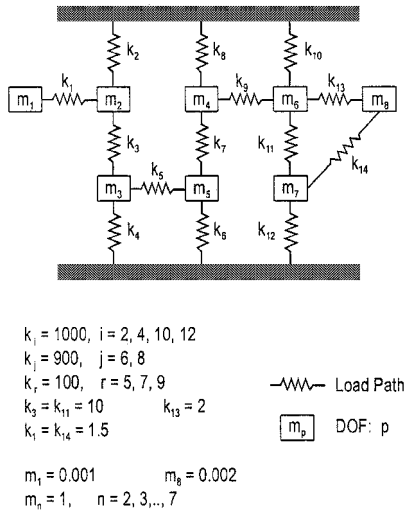

Fig. 3 Kabe's model.[17]

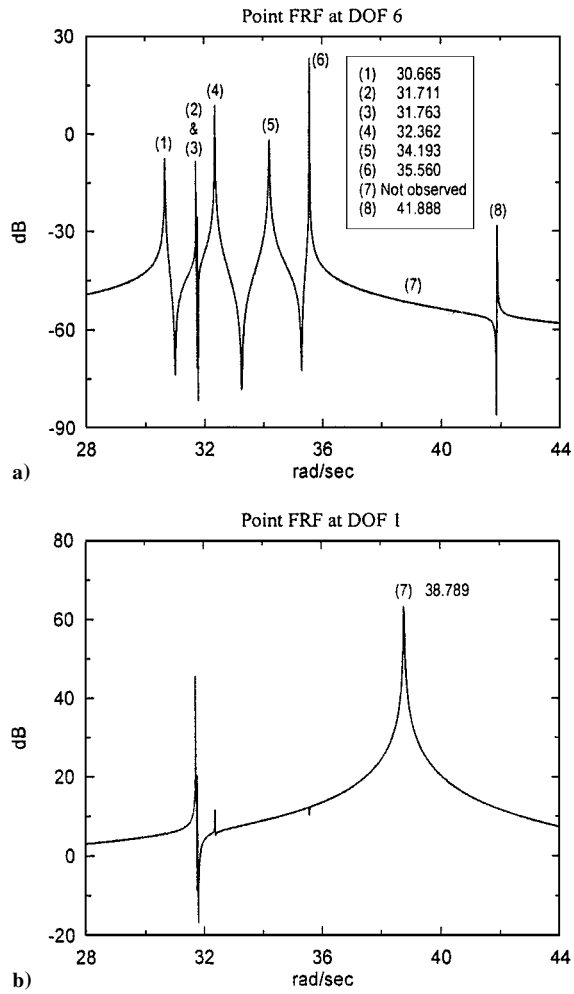

Fig. 4 FRF of Kabe's problem[17] measured at a) m_6 and b) m_1.

by calculating the poles and zeros of all possible damage combinations. Because of the complexity of system dynamics, the change of all poles and zeros measured at m_i, $i = 2, \ldots, 7$, are used as the input of the diagnosis network. A [50–70–6] network is employed to learn the implicit input–output relationship from the training data. Then a set of testing data corresponding to the stiffness loss of from 5 to 35% with 10% intervals is applied to examine the generalization ability of the trained network. After some iteration, the [50–70–6] network has successfully learned the system dynamics. The identification results for testing patterns are depicted in Fig. 5,

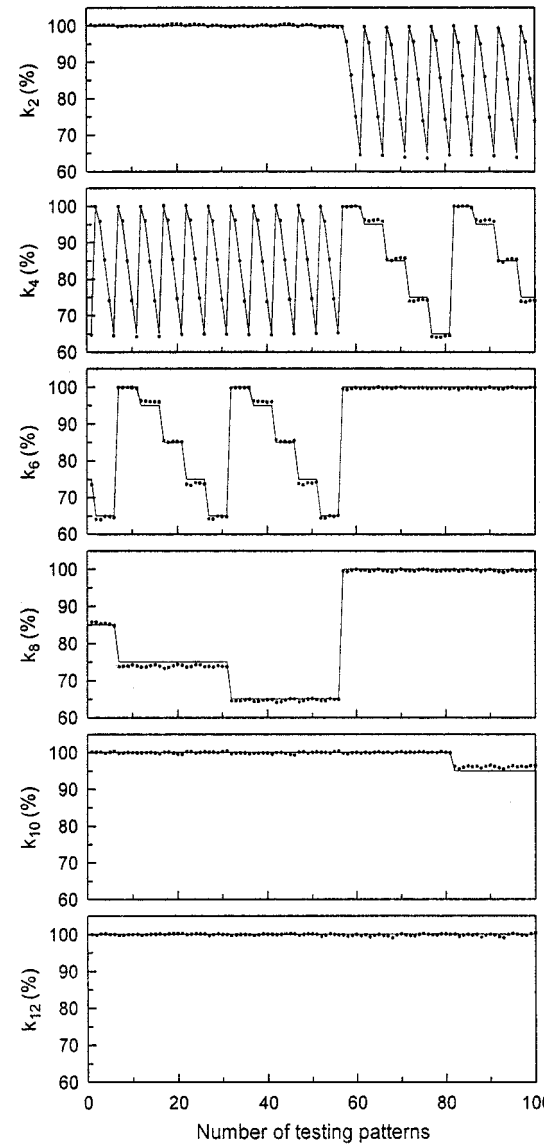

Fig. 5 Structural damage identification of Kabe's problem[17]: ——, desired output, and · · · · , predicted output of [50–70–6] and [36–50–6] diagnosis network; both predictions are almost identical.

where the diagnosis network can also be generalized to predict accurately the unseen damage conditions. The discrepancy between the neural network identification and the desired output is within 1.7%.

To further demonstrate the effectiveness of structural damage identification using pole/zero dynamics, another [36–50–6] network utilizing only the change of the first six poles and the first five zeros is constructed and successfully trained. This simplified diagnosis network also achieves excellent performance similar to that in Fig. 5. Structural damage identification using pole/zero dynamics in a neural network not only avoids the complicated algorithms in traditional model-based schemes, but also provides faster diagnosis results.

IV. Conclusions

1) Structural damage identification by using only the change of natural frequencies is shown to be inadequate because it often leads to ambiguous damage conditions. There can be two distinct damage conditions that have similar, if not exactly the same, changes of natural frequencies. In this Note, an improved method utilizing both poles and zeros in a backpropagation neural network is developed.

2) Kabe's problem[17] is employed to demonstrate the effectiveness in structural damage identification. Both [50–70–6] and [36–50–6] diagnosis networks are shown to identify successfully the damage

conditions of the system with closely spaced natural frequencies. The network performance is excellent in predicting the damage conditions accurately and efficiently, and the discrepancy between the network identification results and the desired output is within 1.7%.

3) In structural damage identification, this method allows one to have the option of selecting one or a few measurements in modal testing for the change of pole/zero as the input data of a diagnosis network. Compared with earlier work carried out by measuring the structural mode shapes, this method significantly simplifies the experimental loads in identifying the extent and location of complex damage conditions. Note that a comprehensive, complete, and relevant set of training data obtained either from numerical simulation or from modal testing for different damage scenarios is the basis of the neural-based scheme. The accuracy of the diagnosis network is usually proportional to the training cost. Further work may be necessary to reduce the required training data without degrading the network performance.

References

[1]Kudva, J. N., Munir, N., and Tan, P. W., "Damage Detection in Smart Structures Using Neural Networks and Finite-Element Analyses," *Smart Materials and Structures*, Vol. 1, 1992, pp. 108–112.

[2]Worden, K., Ball, A. D., and Tomlinson, G. R., "Fault Location in a Framework Structure Using Neural Networks," *Smart Materials and Structures*, Vol. 2, 1993, pp. 189–200.

[3]Szewczyk, Z. D., and Hajela, P., "Damage Detection in Structures Based on Feature-Sensitive Neural Networks," *Journal of Computing in Civil Engineering*, Vol. 8, pp. 163–178.

[4]Barai, S. V., and Pandey, P. C., "Performance of the Generalized Delta Rule in Structural Damage Detection," *Engineering Applications of Artificial Intelligence*, Vol. 8, 1995, pp. 211–221.

[5]Pandey, P. C., and Barai, S. V., "Multilayer Perceptron in Damage Detection of Bridge Structures," *Computers and Structures*, Vol. 54, 1995, pp. 597–608.

[6]Elkordy, M. F., Chang, K. C., and Lee, G. C., "A Structural Damage Neural Network Monitoring System," *Microcomputers in Civil Engineering*, Vol. 9, 1994, pp. 83–96.

[7]Ceravolo, R., Stefano, A. D., and Sabia, D., "Hierarchical Use of Neural Techniques in Structural Damage Recognition," *Smart Materials and Structures*, Vol. 4, 1995, pp. 270–280.

[8]Chen, S. S., and Kim, S., "Automated Signal Monitoring Using Neural Networks in a Smart Structural System," *Journal of Intelligent Materials Systems and Structures*, Vol. 6, 1995, pp. 508–515.

[9]Molas, G. L., and Yamazaki, F., "Neural Networks for Quick Earthquake Damage Estimation," *Earthquake Engineering and Structural Dynamics*, Vol. 24, 1995, pp. 505–516.

[10]Rhim, J., and Lee, S. W., "A Neural Network Approach for Damage Detection and Identification of Structures," *Computational Mechanics*, Vol. 16, 1995, pp. 437–443.

[11]Tsou, P., and Shen, M.-H. H., "Structural Damage Detection and Identification Using Neural Networks," *AIAA Journal*, Vol. 32, No. 1, 1994, pp. 176–183.

[12]Kirkegaard, P. H., and Rytter, A., "The Use of Neural Networks for Damage Detection and Isolation in a Steel Member," *Proceedings of Neural Networks and Combinatorial Optim. in Civil and Structural Engineering*, Civil-Comp Press, Edinburgh, Scotland, U.K., 1993, pp. 1–9.

[13]Islam, A. S., and Craig, K. C., "Damage Detection in Composite Structures Using Piezoelectric Materials," *Smart Materials and Structures*, Vol. 3, 1994, pp. 318–328.

[14]Kaminski, P. C., "The Approximate Location of Damage Through the Analysis of Natural Frequencies with Artificial Neural Networks," *Journal of Process Mechanical Engineering*, Vol. 209, 1995, pp. 117–123.

[15]Ferregut, C. M., Osegueda, R. A., and Ortiz, J., "Artificial Neural Networks for Structural Damage Detection and Classification," *Proceedings of SPIE–The International Society for Optical Engineering*, Vol. 2446, 1995, pp. 68–80.

[16]Yang, S. M., and Lee, G. S., "Vibration Control of Smart Structures by Using Neural Networks," *Journal of Dynamic Systems, Measurement and Control*, Vol. 119, No. 1, 1997, pp. 34–39.

[17]Kabe, A. M., "Stiffness Matrix Adjustment Using Mode Data," *AIAA Journal*, Vol. 23, 1985, pp. 1431–1436.

G. A. Kardomateas
Associate Editor

Noncontact Electron Gun Strain Control of Piezoceramics

George C. Nelson* and John A. Main†
University of Kentucky, Lexington, Kentucky 40506-0108

Introduction

STRAIN control in piezoceramics requires the application of external electric fields to the active material. This has traditionally been accomplished by sandwiching the material between conducting electrodes. The electrodes are appropriately segmented to control individual areas of the actuator (Fig. 1). Although effective, there are definite constraints on using electrodes to accomplish strain control in piezoelectric materials. Application of electric fields to piezoelectric materials in this way may become impractical as the controlled area increases and the spatial resolution becomes finer. In such cases the number of electrodes and leads will become very large.

One possible solution to this problem is to deposit control charges directly onto the surface of the piezoelectric material with an electron gun. An obvious advantage of this method, if it proves to be practical, is that only the electron beam size and the properties of the driven structure will limit spatial resolution.

The idea of applying control charges with an electron gun to stimulate piezoelectric response was put forth in an invention description by Brown and Sivyer.[1] They outlined the design of an acoustic transducer that uses an electron gun to excite a piezoelectric layer. This work stressed dynamic excitation of the piezoelectric material structure rather than strain control. More recently Hubbard[2] described an electron gun system to actuate a wavefront correction mirror constructed from a glass/polyvinylidene fluoride (PVDF) laminate. This is the work most directly relevant to the current investigation because strain control of the piezoelectric structure was emphasized. Hubbard's control method is described and compared to the method used in this investigation in the following technical description.

The most attractive feature of electron gun control is the absence of the constraining electrode pattern in the structure. In theory the electron gun can apply a charge distribution of any size and shape to any location on a distributed structure. This is a significant advantage when extremely large active or smart structures are under consideration for precision applications. The ability to build an active structure without electrode patterns and lead wires greatly increases the options open to the system designer.

If a practical method of shape control of large surfaces with fine spatial resolution is developed a number of applications suggest themselves. Possibilities abound in the areas of acoustics and instrumentation. A particularly intriguing application is large optical mirror structures for space applications. If an extremely precise active structural system capable of maintaining a desired shape to optical tolerances could be constructed, then space telescope mirrors of enormous size might be possible. The flexible nature of electron gun control may make it possible to construct these structures in segments and assemble them on orbit, or perhaps stow them as a furled thin film and deploy them and then tune the structure to a precise optical shape. This is, of course, an extremely bold proposal, and proving such a concept feasible is a task well beyond the scope of the work described herein. This Note is intended only to begin the understanding of the important physics associated with electron gun control of piezoelectric strains.

Received 16 August 1999; revision received 16 October 2000; accepted for publication 6 April 2001.

*Research Assistant, Department of Mechanical Engineering, 521 CRMS Building. Member AIAA.

†Associate Professor, Department of Mechanical Engineering, 521 CRMS Building. Member AIAA.